International Journal of Marine Science and Technology, vol. 2, no. 2, pp. 8–15, 2026 e-ISSN: 3093-3609
http://doi.org/10.65154/ijmst.54 https://i-jmst.vimaru.edu.vn

Numerical Investigation of Hydrodynamic Resistance of Small Passenger Vessels for Inland Waterway Tourism in Vietnam under Calm Water Conditions

Van Diem Le and Van Tung Dam*

Abstract: In many inland waterway tourism destinations in Vietnam, passenger transportation still relies on traditional rowing boats or small motorized vessels, whose operational efficiency and environmental performance remain limited. This study presents a CFD-based investigation of the hydrodynamic resistance characteristics of a representative small passenger vessel intended for inland tourism under calm-water conditions. The hull model was developed from surveyed vessel types currently operating in Vietnamese inland tourism areas, and its performance was evaluated over a practical service-speed range of 2.0–4.0 m/s, corresponding to the displacement, transition, and lower semi-planing regimes. The numerical simulations employed a two-phase air–water model together with a dynamic fluid–body interaction approach to capture free-surface flow and vessel motions. The results show that total resistance increases from approximately 160 N at 2.0 m/s to 578 N at 4.0 m/s, while the resistance coefficients indicate that the residual component remains dominant and the influence of pressure-related and wave-making effects becomes increasingly significant with speed. Additional analysis of wave patterns and hull-surface pressure distribution provides physical insight into the hydrodynamic mechanisms governing the resistance behavior. The obtained results contribute to establishing a baseline hydrodynamic reference for representative inland passenger vessels and provide a practical basis for preliminary propulsion-power estimation and initial electric-propulsion selection for sustainable inland tourism applications.

Keywords: CFD simulation, electric propulsion, hydrodynamic resistance, inland waterway tourism, small passenger vessels.

1. INTRODUCTION

In recent years, inland waterway tourism in Vietnam has grown rapidly, particularly in ecologically sensitive destinations such as Trang An (Ninh Binh Province) and Ba Be Lake (Thai Nguyen Province). Passenger transportation in these areas is currently carried out mainly by traditional rowing boats or vessels powered by internal combustion engines. While rowing boats are environmentally friendly and preserve local cultural values, their operational efficiency is limited due to their reliance on human labor. In contrast, diesel-powered vessels improve transportation efficiency but generate noise, exhaust emissions, and other environmental impacts on inland aquatic ecosystems.

In this context, the transition toward electric-powered tourist vessels has emerged as a promising solution to balance operational efficiency with environmental sustainability. However, for small passenger vessels operating in shallow inland waterways, hydrodynamic resistance becomes a key factor influencing energy efficiency and propulsion power requirements. The magnitude of resistance directly affects battery capacity, operational range, and the feasibility of electric propulsion systems.

Most existing studies on the hydrodynamic performance of small vessels have focused on high-speed craft, planing or semi-planing hulls, and specific resistance-reduction measures under particular geometric and operating conditions. Experimental and numerical investigations have been reported for full-scale and model-scale planing or semi-planing craft [1–5], while CFD-based approaches have also been widely applied to evaluate calm-water resistance, free-surface flow, and vessel motions for various hull configurations, including high-speed monohulls and multihulls [10–13]. These

Manuscript received March 11, 2026; received in revised form March 31, 2026; accepted April 14, 2026; available online June 30, 2026.

Van Diem Le and Van Tung Dam are with the Faculty of Marine Engineering, Vietnam Maritime University, Haiphong, Vietnam (e-mails: diemlv.mtb@vimaru.edu.vn and tungdv.mtb@vimaru.edu.vn).
* Corresponding author.

Research article

studies have contributed significantly to the understanding of wave-making, pressure distribution, and resistance behavior of fast craft over moderate-to-high Froude number ranges.

However, for typical inland passenger vessels currently operating in Vietnamese inland tourism areas, such as Trang An and Ba Be Lake, service speeds are generally relatively low to satisfy both sightseeing requirements and ecological protection. Under these operating conditions, the resistance characteristics are governed primarily by frictional effects, pressure-related resistance, and free-surface interaction associated with the hull geometry, draft, and wetted surface area. Compared with high-speed recreational or planing craft, the hydrodynamic characteristics of such small inland passenger vessels have received much less attention in the existing literature. In addition, many previous CFD studies have considered idealized benchmark hulls or specialized fast-vessel configurations, whereas representative inland passenger hulls derived from surveyed vessels in actual tourism waterways have rarely been investigated in a systematic manner. Furthermore, the connection between calm-water hydrodynamic performance and preliminary electric-propulsion implications for this class of vessels remains only limitedly discussed.

Despite the progress reported in previous studies, a clear gap remains in the hydrodynamic assessment of representative small inland passenger vessels operating at practical tourism service speeds. In particular, systematic CFD-based investigations of hulls derived from surveyed vessels in actual Vietnamese inland tourism waterways remain very limited, especially when the analysis is extended beyond resistance prediction to include flow-field interpretation and preliminary propulsion implications.

Therefore, this study investigates the calm-water hydrodynamic resistance of a representative small inland passenger vessel proposed as a replacement for traditional rowing boats in Vietnamese tourism waterways. The novelty of this work lies in its focus on a practically significant yet insufficiently documented vessel category that is widely deployed in Vietnam and plays a key role in the transition toward sustainable inland waterway transport. A numerical approach based on computational fluid dynamics (CFD), coupled with a Dynamic Fluid–Body Interaction (DFBI) model, is employed to predict both resistance and free-motion responses over a practical operating speed range of 2.0–4.0 m/s. This range corresponds to the transition from the displacement regime to the semi-planing regime, as characterized by the Froude number based on the vessel waterline length. The results provide a baseline hydrodynamic reference for this class of inland passenger vessels and establish a practical foundation for preliminary propulsion power estimation and the initial selection of electric propulsion systems in sustainable inland tourism applications.

The specific contribution of the present study is the establishment of a baseline hydrodynamic reference for a representative small inland passenger vessel hull, developed from a survey of vessels currently operating in Vietnamese tourism waterways. The results obtained elucidate the resistance characteristics over a practical service-speed range and provide a reliable foundation for preliminary propulsion power estimation, as well as for the initial selection of electric propulsion systems.

2. THEORETICAL BACKGROUND

In the hydrodynamic analysis of ships operating in calm water, it is necessary not only to determine the total resistance but also to evaluate dimensionless parameters that characterize the flow regime. Among these parameters, the Froude number is one of the most important. The Froude number represents the ratio between inertial forces and gravitational forces and reflects the degree of wave formation generated by a moving vessel. It is defined as follows

$$Fr = \frac{v}{\sqrt{gL}} \tag{1}$$

where v is the ship speed, g is the gravitational acceleration, and L is the waterline length.

For vessels operating in calm water, the Froude number determines the nature of the wave-making process and directly influences the pressure distribution around the hull. As the Froude number increases, wave generation becomes more significant, leading to a noticeable increase in the pressure resistance component of the total hydrodynamic resistance.

Based on the Froude number, the operating speed of a vessel can be classified into different hydrodynamic regimes. According to previous studies, vessels with $Fr < 0.4$ typically operate in the displacement regime, where the vessel is primarily supported by buoyancy forces. In the range of $0.4 \le Fr \le 0.65$, the vessel enters the semi-displacement regime, where wave-making effects become increasingly significant. When the Froude number increases further to approximately $0.65 < Fr \le 1.0$, the vessel begins to operate in the semi-planing regime, in which hydrodynamic lift starts to contribute to supporting the vessel weight. For $Fr > 1.0$, the vessel is generally considered to operate in the planing regime [4, 5].

Considering the overall hydrodynamic forces acting on the hull during forward motion, the total hydrodynamic resistance R_T in the longitudinal direction is primarily composed of two main components (2): pressure resistance R_P and frictional resistance R_F. Pressure resistance is associated with the pressure distribution around the hull and is mainly influenced by the formation of the free-surface wave system and flow separation near the bow and stern regions. As vessel speed increases, wave generation becomes more pronounced, leading to a significant growth of the pressure resistance component. In contrast, frictional resistance originates from viscous shear stresses acting along the wetted surface of the hull due to the relative motion between the fluid and the hull surface. This component is strongly dependent on the wetted surface area, hull geometry, and flow velocity. The combined contribution of these two components determines the total hydrodynamic resistance (N) experienced by the vessel during operation [6, 7] is given by

(a) Traditional rowing boats in Trang An, Ninh Binh.

b) Motorized boats in Ba Be Lake, Thai Nguyen.

Fig. 1. Typical passenger vessels used in inland waterway tourism in Vietnam.

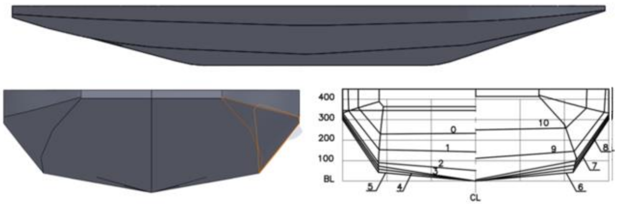

Fig. 2. Hull design vessel model.

$$R_T = R_P + R_F \qquad (2)$$

In addition to dimensional resistance, hydrodynamic performance is often expressed in non-dimensional form using the total resistance coefficient. According to artice [8] and the International Towing Tank Conference [9], the total resistance coefficient is defined as

$$C_T = \frac{R_T}{0,5\rho S V^2} \qquad (3)$$

where ρ denotes the water density, S is the wetted surface area, and V indicates the vessel speed. This coefficient is useful for comparing resistance characteristics under different operating conditions and with published benchmark data.

For preliminary propulsion-power estimation, the effective power (W) associated with the total hydrodynamic resistance may be expressed as

Table 1. Main characteristics of the vessel.

Parameters	Value	Unit
Length over all	4.54	m
Length at waterline	3.48	m
Beam	1.30	m
Beam at waterline	1.19	m
Depth moulded	0.45	m

$$P_E = R_T V \qquad (4)$$

For practical propulsion-system assessment, the required input power (W) may be estimated as

$$P = \frac{R_T V}{\eta} \qquad (5)$$

where η is the overall propulsion-system efficiency.

3. VESSEL MODEL

Based on a survey of the hull geometry, principal dimensions, and operational conditions of vessels commonly used in ecological tourism areas within Vietnam's inland waterways, a representative ship hull model was developed for hydrodynamic investigation. Typical surveyed vessel types are illustrated in Fig. 1a and Fig. 1b, representing traditional rowing boats in Trang An and motorized tourist boats in Ba Be Lake, respectively. The model was designed with the objective of optimizing operational performance for ecological tourism while maintaining geometric similarity to vessels currently used in inland tourist waterways. The principal dimensions of the vessel were selected based on typical passenger boats operating in these two areas to ensure that the model represents realistic operating conditions, and the main characteristics of the designed vessel are summarized in Table 1.

The designed representative hull form is shown in Fig. 2. Accordingly, the hull model was designed as a monohull configuration with a shallow-draft bottom form incorporating a deadrise angle of 18°, making it suitable for operation in inland waterways with limited water depth while providing a more streamlined underwater geometry for hydrodynamic assessment. This hull form was not intended as an exact geometric replica of traditional flat-bottom rowing boats, but rather as a representative inland passenger vessel configuration derived from surveyed boats currently operating in Vietnamese tourism waterways. The bow section was designed with a slender shape to reduce pressure resistance and mitigate wave generation in the low-speed operating regime, while the stern section was streamlined to improve wake development behind the hull and to reduce the size of the stern vortex region.

To reflect the practical operating conditions of inland tourist vessels, the hydrodynamic behavior of the vessel was analyzed within a speed range of 2.0–4.0 m/s. This range represents the typical service speeds encountered in inland tourism operations, including low-speed

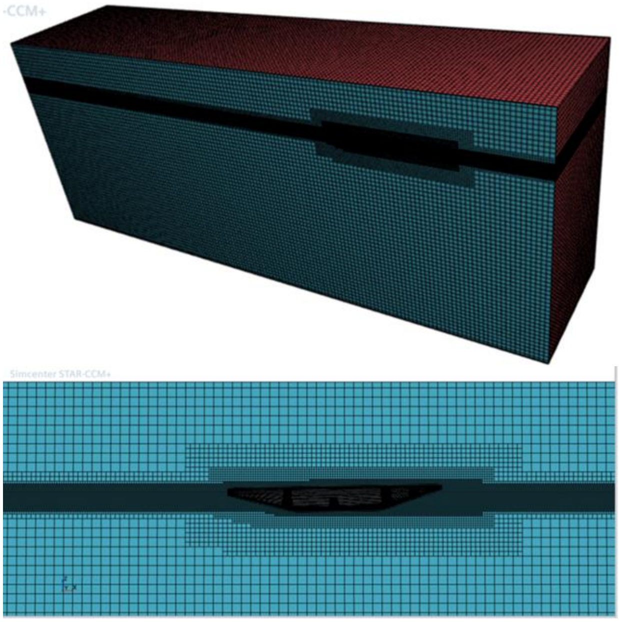

Fig. 3. The computational mesh used in the CFD simulation.

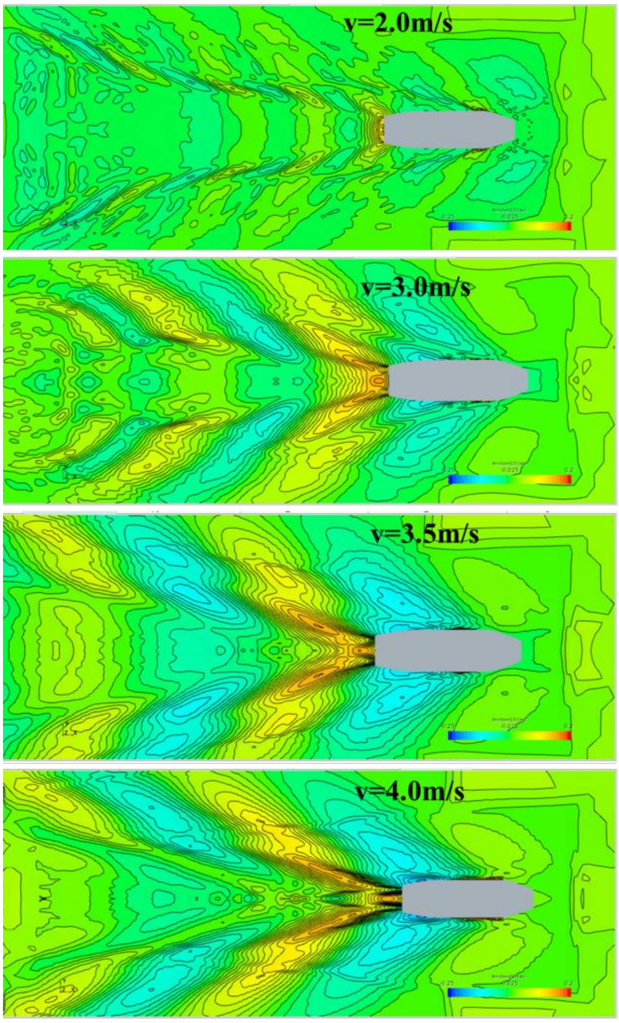

Fig. 4. The wave pattern around the vessel at different operating speeds.

cruising during sightseeing activities and higher transit speeds when the vessel moves between passenger

Table 2. Mesh convergence results at v=3.5 m/s.

Mesh level	**Number of cells (million)**	R_T **(N)**	$C_T \times 10^3$
Coarse	2.602	491	20.09
Medium	3.671	483	19.81
Fine	5.171	482	19.77

Table 3. Hydrodynamic resistance and resistance coefficients at different vessel speeds.

v **m/s**	***FR***	S **(m²)**	R_T **(N)**	$C_T \times 10^3$	$C_F \times 10^3$	$C_R \times 10^3$
2.0	0.342	4.20	160	19.05	3.20	15.85
2.5	0.428	4.12	211	16.39	3.07	13.31
3.0	0.513	4.03	358	19.74	2.98	16.67
3.5	0.599	3.96	483	19.91	2.90	17.01
4.0	0.685	3.90	578	18.53	2.83	15.69

Table 4. Comparison of CFD results with NSS data.

Study	v **(m/s)**	***Fr***	S **(m²)**	$C_T \times 10^3$	$C_R \times 10^3$
Present study	3.0	0.513	4.03	19.74	16.67
NSS (C4 bare hull)	2.5	0.515	1.17	9.34	7.44
Present study	3.5	0.599	3.96	19.91	17.01
NSS (C4 bare hull)	3.0	0.618	1.14	7.9	6.22

boarding and disembarking locations.

The investigated speed range represents different hydrodynamic operating conditions of the vessel. At lower speeds of approximately 2.0–2.5 m/s, the vessel operates primarily in the displacement regime, where buoyancy remains the dominant supporting force and the generated wave system is relatively moderate. As the speed increases to around 3.0–4.0 m/s, the hydrodynamic characteristics gradually change toward the semi-displacement and semi-planing regime. In this range, wave-making effects become more pronounced and the pressure resistance component contributes more significantly to the total resistance.

Evaluating the resistance characteristics across this operating speed range allows the influence of vessel speed on the total hydrodynamic resistance to be systematically assessed. The findings also provide an important basis for estimating the required propulsion power and for selecting an appropriate electric propulsion system for small inland passenger vessels designed for sustainable tourism operations.

4. NUMERICAL SETUP

To evaluate the hydrodynamic resistance

characteristics of the vessel model, Computational Fluid Dynamics (CFD) simulations were performed using STAR-CCM+. The simulations were carried out under calm-water conditions to determine the total resistance of the hull and to analyze the flow field characteristics around the vessel at the selected operating speeds.

The computational domain was defined as a rectangular box surrounding the vessel hull. The inlet boundary was located at a distance of $2L_{WL}$ upstream of the bow to ensure a fully developed flow before reaching the hull, while the outlet boundary was positioned $15L_{WL}$ downstream of the stern to allow sufficient development of the wake and wave system behind the vessel. The side, top, and bottom boundaries were placed at distances of $6L_{WL}$, $3L_{WL}$, and $6L_{WL}$ from the hull, respectively, in order to minimize the influence of boundary conditions on the simulation results. A velocity inlet condition was applied at the inlet boundary, whereas a pressure outlet condition was specified at the outlet boundary. The hull surface was modeled as a no-slip wall boundary, while the lateral boundaries and the center plane were assigned symmetry boundary conditions to reduce computational cost by exploiting the symmetry of the problem [1, 9, 10]. This domain configuration was adopted for a baseline hydrodynamic resistance assessment under calm-water conditions, rather than to explicitly reproduce shallow-water bottom effects or squat-related channel-bed interaction. On this basis, the bottom boundary was positioned sufficiently far from the hull to limit artificial confinement effects, while the downstream outlet was extended to ensure adequate development of the stern wake and free-surface wave system before reaching the outlet boundary.

The computational mesh was generated with variable cell density across the computational domain to ensure both numerical accuracy and computational efficiency. Mesh refinement was applied in the free-surface region as well as near the bow and stern in order to accurately capture wave generation and the flow features around the hull. In contrast, coarser meshes were used in regions farther away from the vessel to reduce computational cost The computational mesh used in the CFD simulation is shown in Fig. 3.

To assess the reliability of the numerical predictions, a grid convergence study was carried out using three mesh levels, namely coarse, medium, and fine. The corresponding grid sizes consisted of approximately 2.60, 3.67, and 5.17 million cells, respectively. The mesh refinement was performed with a refinement ratio of $\sqrt{2}$ between successive grid levels [9, 10]. The grid convergence results for the case at a vessel speed of 3.5 m/s are summarized in Table 2. As the mesh density increases, both the predicted total resistance and the corresponding resistance coefficient show a clear convergence trend, indicating a reduction in numerical discretization error. In particular, the relative difference between the coarse and medium grids is 1.63%, whereas the discrepancy between the medium and fine grids is reduced to only 0.21%. This small variation indicates that the numerical solution becomes only weakly sensitive to further mesh refinement beyond the medium grid. Therefore, the medium mesh was selected for the subsequent simulations as a practical compromise between numerical accuracy and computational efficiency.

The flow field was solved using the Reynolds-Averaged Navier–Stokes (RANS) equations for incompressible flow, coupled with the Volume of Fluid (VOF) method to capture the air–water free surface. Vessel motions were modeled through the DFBI approach with two degrees of freedom, namely heave and pitch. An unsteady simulation framework was adopted in order to resolve both the air–water free-surface evolution and the coupled vessel motions described by the VOF and DFBI models. Turbulence was represented using the Realizable k–ε Two-Layer model together with the Two-Layer All y+ wall treatment, providing a practical balance between numerical robustness, computational efficiency, and near-wall resolution for resistance-oriented CFD simulations. For the selected medium mesh, the wall y+ values along the hull surface were also examined for representative low- and high-speed conditions. The results indicate that the wall y+ remained within approximately 5–31 at 2.0 m/s and 8.6–41.5 at 4.0 m/s. These ranges are considered compatible with the adopted Two-Layer All y+ wall treatment and indicate that the near-wall resolution is adequate for the present resistance-oriented CFD simulations.

The time-step size was determined according to the ITTC recommended guideline, Δt=0.005–0.01L/U. For the present vessel and operating-speed range, this corresponds to approximately 0.004–0.017 s; therefore, a constant time step of 0.005 s was adopted to ensure stable free-surface evolution and reliable prediction of vessel motions and resistance throughout the simulations [9-13]. The simulations were performed over a physical time of 10 s, corresponding to 2000 time steps. The total number of solver iterations was approximately 25000, which corresponds to about 12–13 inner iterations per time step on average. Numerical convergence was monitored through the residual histories together with the stabilization of the predicted total resistance and the vessel motions in heave and pitch.

5. RESULTS AND DISCUSSION

5.1. Free-surface wave pattern

The free-surface elevation and wave patterns generated by the vessel within the investigated speed range of 2.0–4.0 m/s are presented in Fig. 4. The simulation results reveal the development of a characteristic wave system behind the hull, consisting of transverse waves and divergent waves propagating from the bow region toward both sides of the flow field. The characteristics of the free-surface deformation vary noticeably depending on the hydrodynamic regime corresponding to each operating speed range.

Within the lower vessel-speed range of 2.0–2.5 m/s, the deformation of the free surface remains relatively small. The generated waves exhibit low amplitudes and the wake system behind the vessel is still weakly developed. Under these conditions, buoyancy is the dominant supporting force acting on the vessel, and the

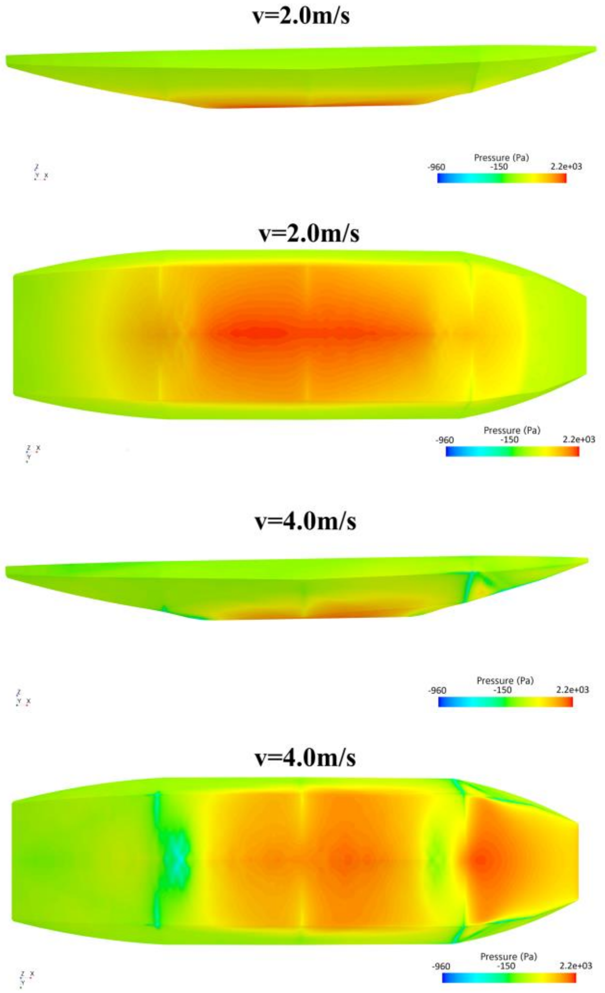

Fig. 5. Pressure distribution on the hull surface at representative operating speeds 2.0 m/s and 4.0 m/s.

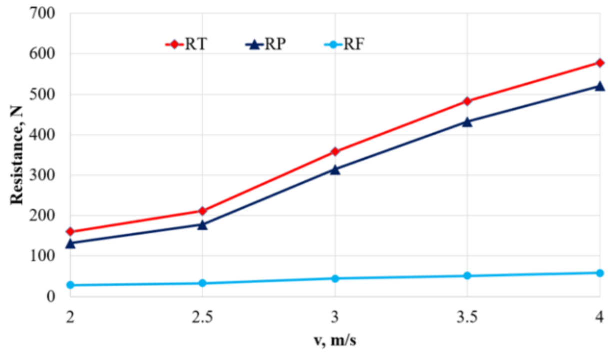

Fig. 6. Dependence of hydrodynamic resistance on vessel speed.

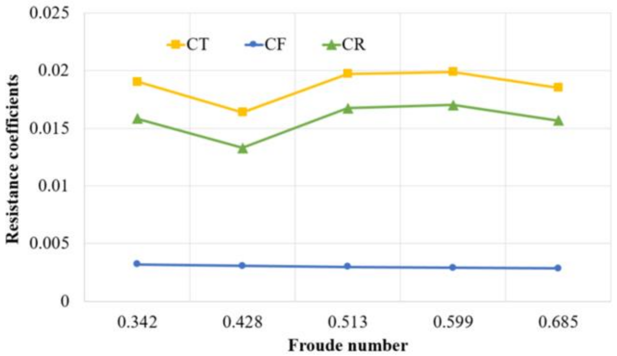

Fig. 7. Dependence of resistance coefficients on Froude number.

interaction between the hull and the free surface is still limited. As a result, the contribution of wave-making resistance to the total hydrodynamic resistance remains relatively small.

As the vessel speed increases to the semi-displacement or transition regime (2.5–3.5 m/s), the interaction between the hull and the free surface becomes more pronounced. The density of contour lines around the bow and stern regions increases significantly, indicating stronger pressure gradients and enhanced wave generation. The divergent wave branches become more visible and extend further away from the vessel centerline. At the same time, the transverse waves behind the stern begin to form a more structured wake system, reflecting the increasing importance of wave-making effects in the overall hydrodynamic behavior of the vessel.

When the vessel speed reaches 4.0 m/s, corresponding to the semi-planing regime, the deformation of the free surface becomes considerably stronger. The wave system behind the vessel develops more clearly, and the Kelvin wake pattern becomes more distinct. This indicates that a larger portion of the vessel's kinetic energy is transferred to the free-surface wave system. In this regime, hydrodynamic lift begins to contribute partially to supporting the vessel weight, while the pressure resistance component increases significantly due to the stronger interaction between the hull and the surrounding flow field.

5.2. Pressure distribution on the hull surface

The pressure distribution on the hull surface at 2.0 and 4.0 m/s (Fig. 5) reveals a clear modification of the hydrodynamic loading pattern as the vessel speed increases from the displacement regime toward the transitional and lower semi-planing regimes. At 2.0 m/s (Fr = 0.342), the pressure field remains relatively smooth, characterized by a broad positive-pressure region along the lower hull and moderate pressure gradients over the wetted surface, indicating that the vessel is primarily supported by hydrostatic buoyancy.

At 4.0 m/s (Fr = 0.685), the pressure contours become increasingly non-uniform, with a more concentrated positive-pressure region beneath the forward-bottom area and more pronounced localized low-pressure zones near the bottom–side transition and the tapered aft region. This redistribution of pressure indicates enhanced local flow acceleration and deceleration, reflecting a stronger dynamic interaction between the hull and the free surface at higher speed. Under these conditions, the coupled heave and pitch motions become more significant and contribute more noticeably to the overall hydrodynamic response of the vessel

Consequently, dynamic pressure effects play an increasingly important role in hull support and in the growth of pressure resistance, which is further reflected in the hydrodynamic resistance results.

5.3. Hydrodynamic resistance

The calculated hydrodynamic resistance shows a clear increasing trend with vessel speed within the investigated range of 2.0–4.0 m/s, as illustrated in Table 3 and Fig. 6. Specifically, the total resistance increases from approximately 160N at 2 m/s to about 578N at 4 m/s, with intermediate values of 211N, 358N, and 483N corresponding to speeds of 2.5 m/s; 3 m/s; and 3.5 m/s, respectively.

This increase in resistance with vessel speed reflects the growing contribution of wave-making effects to the total hydrodynamic resistance. At lower speeds, the vessel mainly operates in the displacement regime, where viscous effects dominate and wave generation remains moderate. As the speed increases, the interaction between the hull and the free surface becomes stronger, leading to a more developed wave system and a rapid increase in the pressure resistance component.

In addition to the dimensional resistance results, the resistance coefficients in Fig. 7 indicate that the residual component remains dominant over the investigated speed range, while the frictional component varies more moderately with speed. This suggests that the increase in total resistance is governed mainly by pressure and wave-making effects. A more detailed reliability assessment based on the resistance decomposition and benchmark comparison is presented in Section 5.4.

The obtained resistance results also provide a basis for estimating the required propulsion power and for the preliminary selection of an electric propulsion system. Based on the predicted resistance over the investigated speed range, the required input power is estimated to be approximately 0.53–3.85 kW, assuming an overall propulsion-system efficiency of 0.6. This suggests that an electric motor with a rated power of about 4.0–5.0 kW may be suitable for the present vessel under calm-water conditions. It should be noted, however, that the assumed overall efficiency is used here as a preliminary design-level approximation and does not explicitly separate losses associated with motor controllers, battery conversion, mechanical transmission, and auxiliary onboard systems. Therefore, the resulting propulsion-power estimates should be interpreted as preliminary guidelines for early-stage electric-propulsion selection rather than as definitive full-system design values.

5.4. Model Reliability Assessment

The reliability of the CFD predictions was evaluated through a resistance decomposition approach based on the ITTC correlation line, complemented by a benchmark-oriented comparison with data from the Naples Systematic Series (NSS) [9, 14]. In this context, the comparison is conducted as a plausibility assessment over a corresponding Froude-number range, rather than as a direct validation against a geometrically identical hull form. The investigated operating regime (Fr = 0.34–0.68) spans a range of increasing vessel speeds, within which progressive variations in wave patterns and total resistance characteristics are observed.

The total resistance coefficient (C_T) obtained from CFD simulations was decomposed into frictional resistance (C_F) estimated from the ITTC correlation line and residual resistance (C_R), calculated as $C_R = C_T - C_F$ [9]. The results show that C_F slightly decreases with increasing speed, while C_R remains dominant throughout the investigated range. This indicates that pressure and wave-making effects govern the resistance characteristics, which is consistent with the expected hydrodynamic behavior of small inland vessels operating in the displacement-to-transition regime.

To further assess the reliability, the numerical results were compared with the NSS benchmark data for hard-chine hulls in the overlapping Froude-number range. The comparison is summarized in Table 4.

The comparison shows that the present vessel consistently exhibits higher resistance coefficients than the NSS benchmark across the overlapping Froude-number range. At $Fr \approx 0.51$, the total resistance coefficient (CT) increases from 0.00934 for the NSS hull to 0.01974 for the present vessel, while the residual resistance coefficient (CR) rises from 0.00744 to 0.01667 [10]. This trend persists at the higher operating condition, where both CT and CR remain approximately twice those of the NSS reference.

The observed discrepancy is primarily attributed to differences in hull-form characteristics and the resulting hydrodynamic response, rather than to any inconsistency in the CFD predictions. The investigated vessel represents a fuller inland-passenger hull with a lower waterline length-to-beam ratio and a broader wetted footprint, whereas the NSS C4 reference corresponds to a more slender hard-chine series developed for semi-planing and planing craft. As a result, the two hulls do not redistribute pressure, dynamic support, and wave-making effects in the same manner. The present hull tends to retain a larger buoyancy-supported wetted area over the investigated speed range, while the NSS C4 geometry is more favorable to lift-assisted operation and lower residual resistance at comparable Froude numbers.

In the present study, S denotes the wetted hull area corresponding to each simulated operating condition. Its relatively larger magnitude, compared with the NSS benchmark, reflects both the larger absolute dimensions and the fuller hull form of the investigated vessel, while its slight reduction with increasing speed is consistent with the DFBI-predicted heave–pitch response and the associated decrease in the submerged hull area. The frictional resistance coefficient (CF), evaluated using the ITTC correlation line, exhibits a mild decrease with speed due to Reynolds-number effects and should not be interpreted as a reduction in dimensional frictional resistance. Accordingly, the elevated CT and CR values obtained in this study are primarily attributed to enhanced pressure- and wave-related effects associated with the fuller hull geometry.

Overall, the agreement in hydrodynamic trends between CFD predictions and the NSS benchmark confirms the physical plausibility of the numerical results. Although not a direct experimental validation for the specific hull, the comparison supports the reliability of the simulations and their suitability for propulsion power estimation and electric propulsion system selection in calm-water operating conditions.

6. CONCLUSION

This study presents a CFD-based investigation of the hydrodynamic resistance characteristics of a small passenger vessel intended for inland waterway tourism in Vietnam under calm-water conditions. A representative hull form was developed based on a survey of vessels currently operating in inland tourist areas, and its performance was evaluated over a service-speed range of 2–4 m/s, corresponding to the displacement, transitional, and lower semi-planing regimes. The analysis focused on the free-surface wave pattern, hull-surface pressure distribution, and overall resistance characteristics.

The results indicate that vessel speed has a significant influence on the hydrodynamic response. As the speed increases, free-surface deformation becomes more pronounced and the pressure distribution over the hull becomes increasingly non-uniform, reflecting a stronger dynamic interaction between the hull and the free surface. The resistance results show a clear increase in total resistance with speed, while the resistance coefficients reveal that the residual component remains dominant and the frictional component varies more moderately. These findings suggest that the growth in resistance is primarily governed by pressure-related and wave-making effects as the vessel gradually departs from buoyancy-dominated operation.

The results demonstrate a pronounced increase in total hydrodynamic resistance across the investigated operating range, reaching approximately 580 N at the highest service condition, with the residual resistance component remaining dominant in the overall resistance characteristics. Based on these findings, the required propulsion-system input power is estimated to lie in the range of 4–5 kW. These results provide evidence supporting the hydrodynamic feasibility of the proposed vessel concept and underscore the practical relevance of the study for the design and development of inland passenger vessels in Vietnam, particularly in advancing more sustainable inland waterway transport solutions.

Despite the useful contributions of the present study, several limitations should be acknowledged. The numerical analysis was conducted under calm-water conditions within a representative operating-speed range and focused on the resistance characteristics of a single baseline hull derived from surveyed inland passenger vessels. The present setup was adopted for baseline hydrodynamic assessment and therefore does not explicitly account for shallow-water confinement, bottom proximity, squat-related effects, wind, waves, current disturbances, or other unsteady environmental influences that may affect actual inland-vessel operation. In addition, direct experimental validation for the investigated hull has not yet been carried out, and the current assessment remains limited to mesh convergence, empirical resistance decomposition, and comparison with benchmark data.

Nevertheless, the agreement with empirical formulations and benchmark results suggests that the numerical predictions are sufficiently reliable for preliminary design and performance assessment. Future work should include experimental measurements and extended analyses considering shallow-water effects, bottom-proximity and squat-related behavior, the influence of hull-bottom deadrise angle on hydrodynamic characteristics, unsteady operating conditions, and systematic hull-form variation under the same design constraints.

ACKNOWLEDGMENT

This research is funded by Vietnam Maritime University under grant number: DT25-26.29.

REFERENCES

[1] A. G. Avci and B. Barlas, “An experimental and numerical study of a high speed planing craft with full-scale validation,” *Journal of Marine Science and Technology–Taiwan*, vol. 26, no. 5, pp. 617-628, 2018.

[2] M. Sulman et al., “Hydrodynamic performance of high-speed craft: A CFD study on spray rails,” *Journal of Marine Science and Engineering*, vol. 13, no.3, art. no. 438, 2023.

[3] B. Utomo et al., “Hydrodynamic analysis of high-speed vessels in shallow and deep water using CFD,” *Kapal: Jurnal Ilmu Pengetahuan dan Teknologi Kelautan*, vol.20, no. 2, pp.146-153, 2023.

[4] C. Q. Judge and A. M. Ibrahim, “Experimental investigation of motions and global hull girder bending moment of a semi-displacement vessel,” *Ocean Engineering*, vol.320, art. no.120295, 2025.

[5] L. D. Leal-Ruiz et al., “Effect of speed and hull length on the hydrodynamic performance of a semi-planing hull of a shallow-draft watercraft,” *Journal of Marine Science and Engineering*, vol.11, no. 12, pp. 2328, 2023.

[6] A. F. Molland , S. R. Turnock, and D. A. Hudson, *Ship resistance and propulsion*, Cambridge University Press, 2017.

[7] V. Bertram, *Practical ship hydrodynamics*, Elsevier, 2012.

[8] C. Zhang, Y. He, and D. Zhang. "Ship propulsion system," *Encyclopedia of Ocean Engineering*. Springer Nature Singapore, pp. 1645-1653, 2022.

[9] ITTC, “Practical guidelines for ship CFD applications,” ITTC – Recommended Procedures and Guidelines, 7.5-03-02-03, pp. 1-16, 2024.

[10] T. V. Ha, T. N. Tu, and P. M. Ngoc, “Numerical investigation on the motion of a high-speed planning hull in calm water condition using RANSE method,” *IOP Conference Series: Earth and Environmental Science*, vol. 1278, no. 1, art. no. 012022, 2023.

[11] S. Guo, et al. "Numerical study on the influence of catamaran hull arrangement and demihull angle on calm water resistance," *Journal of Marine Science and Engineering* vol. 13, no.4, art. no. 815, 2025.

[12] P. Huang et al., "Numerical investigation on the hydrodynamic response of pentamaran—resistance analysis of different outrigger inclination angles." *Journal of Marine Science and Engineering*, vol.11, no.1, art. no. 186, 2023.

[13] O. Deniz et al. "Full-scale CFD analysis of Double-M craft seakeeping performance in regular head waves." *Journal of Marine Science and Engineering*, vol. 9, no.5, art. no. 504, 2021.

[14] F. De Luca and C. Pensa, “The Naples warped hard chine hulls systematic series,” *Journal of Ocean Engineering*, vol. 139, pp. 205-236, 2017.